LED Model-Driven Reservoir Computing for Signal Equalization in OFDM-VLC System

Yixian Dong, *Member, IEEE*, Yeping Huang, *Graduate Student Member, IEEE*, Xiong Deng, *Senior Member, IEEE*, Songsui Li, *Member, IEEE*, Xihua Zou, *Senior Member, IEEE*, Wei Pan, Peter Bienstman, *Member, IEEE*, and Lianshan Yan, *Senior Member, IEEE*

***Abstract*—This paper introduces a digitally realized, model-driven Reservoir Computing (RC) equalizer for Orthogonal Frequency Division Multiplexing (OFDM) in Visible Light Communication (VLC) systems. The design incorporates a Light Emitting Diode (LED) model building upon the frameworks of Time-Delay Reservoir Computing (TDRC) and Physics-Informed Neural Networks (PINN). In contrast to traditional RC, which uses a randomly connected neural network reservoir, the proposed method integrates a physical model that emulates the nonlinear electro-optical behavior of LEDs into the reservoir layer. This approach directly incorporates the intrinsic characteristics of LEDs, enabling the equalizer to more effectively capture the signal distortions caused by VLC channels. As a result, the model-driven RC significantly improves signal recovery under varying channel conditions, including different bandwidths and modulation voltages. Experimental results show that the proposed method achieves up to 56.0% and 34.6% reductions in Bit Error Rate (BER) compared to traditional RC and Volterra equalizers, respectively. The method also improves average subcarrier Signal-to-Noise Ratio (SNR) by 1.2 dB over Volterra and by 1.5 dB over traditional RC, resulting in an achievable rate improvement by nearly 10%. Additionally, the model-driven RC offers a key advantage in terms of data efficiency for the training stage, requiring only 20% of the total dataset compared to the 50% required by traditional RC and Volterra equalizers.**

***Index Terms*—LED, nonlinear equalization, OFDM, reservoir computing, visible light communication.**

I. Introduction

VISIBLE Light Communication (VLC) is recognized as a key technology for the next generation 6G era [1] due to its significant advantages, including an abundant and unlicensed spectrum as well as enhanced security resulting from its immunity to electromagnetic interference [2]. In addition, VLC systems allow seamless integration with existing lighting infrastructure, which substantially reduces deployment cost and energy consumption. In comparison with Radio Frequency (RF) communication, VLC offers safety advantages in environments where RF emissions must be limited, such as in hospitals and on airplanes. Furthermore, VLC provides high data rates that are well suited for short range and high capacity applications. This makes VLC a promising solution for scenarios such as indoor navigation, secure data transmission, and the Internet of Things (IoT), all of which represent critical applications in the development of 6G networks [3] .

Spectrally efficient modulation schemes are employed in VLC systems to achieve high transmission rates. Advanced techniques, including higher order Quadrature Amplitude Modulation (QAM) and Orthogonal Frequency Division Multiplexing (OFDM), have been widely adopted [4]. OFDM is particularly attractive for high-speed VLC because it improves spectral efficiency and mitigates Intersymbol Interference (ISI) [5]. However, the performance of OFDM-VLC systems becomes increasingly constrained when the modulation bandwidth approaches the intrinsic low-pass limit of LEDs and their linear operating range [6]. Higher modulation orders and data rates intensify the nonlinear characteristics of LEDs, leading to significant degradation in Bit Error Rate (BER). In addition, the inherently high Peak-to-Average Power Ratio (PAPR) of OFDM signals further amplifies the impact of LED nonlinearity, making reliable high-speed transmission more challenging [7], [8].

To mitigate signal distortion in OFDM-VLC systems, both linear and nonlinear equalization techniques have been investigated. One-tap equalization [9] is widely adopted due to its simplicity, but it is ineffective in compensating for nonlinear distortions in OFDM-VLC systems [10], [11], mainly caused by LEDs. Volterra equalizers are capable of mitigating such nonlinearities, but their complex structures and high computational requirements hinder practical deployment [12], [13]. In recent years, neural network based equalization techniques have attracted increasing attention in the optical communication domain. Recurrent Neural Networks (RNN) [14], [15], Radial Basis Function Neural Networks (RBFNN) [16], and Long Short Term Memory (LSTM) networks [17], [18] have demonstrated effectiveness in mitigating nonlinear impairments in optical systems, and they also alleviate the detrimental impact of the PAPR in OFDM-VLC systems [19]. However, the high equalization performance of these neural network models is

Received 19 November 2025; revised 22 January 2026; accepted 7 February 2026. Date of publication 10 February 2026; date of current version 2 May 2026. *(Corresponding author: Yixian Dong.)*

Yixian Dong, Yeping Huang, Xiong Deng, Songsui Li, Xihua Zou, Wei Pan, and Lianshan Yan are with the Key Laboratory of Photonic-Electronic Integration and Communication-Sensing Convergence (Ministry of Education), Southwest Jiaotong University, Chengdu 610031, China (e-mail: ydong@swjtu.edu.cn; hyp@my.swjtu.edu.cn; xiongdeng@swjtu.edu.cn; ssli@swjtu.edu.cn; zouxihua@swjtu.edu.cn; wpan@swjtu.edu.cn; lsyan@home.swjtu.edu.cn).

Peter Bienstman is with Ghent University, 9000 Ghent, Belgium (e-mail: peter.bienstman@ugent.be).

Color versions of one or more figures in this article are available at https://doi.org/10.1109/JLT.2026.3663361.

Digital Object Identifier 10.1109/JLT.2026.3663361

accompanied by considerable architectural complexity, which leads to slower convergence rates and increased optimization difficulty. In particular, the training process requires backpropagation through the entire network to update all parameters, resulting in significant computational overhead and elevated energy consumption [20].

Reservoir Computing (RC) is an innovative recurrent network paradigm that employs a fixed stochastic reservoir to facilitate efficient model training. In RC, the input and recurrent connection weights are randomly generated and remain constant, while only the output weights are trained using simple methods such as ridge regression [21]. This design significantly reduces computational complexity and latency. Moreover, RC shows strong potential in tasks such as time series prediction, signal detection, speech recognition, and real-time classification, due to its ability to model complex dynamics with simple architectures [22], [23], [24], [25]. To implement RC in an analog method, [26] proposed using a single nonlinear node with delayed feedback to emulate the dynamics of a high-dimensional system, thereby replacing the need for a large number of physical nodes. This concept laid the foundation for various photonic Time-delay RC (TDRC) implementations, including those based on Vertical-Cavity Surface-Emitting Lasers (VECSELs), semiconductor lasers, and microring resonators [27], [28].

The performance of RC, similar to other data-driven neural networks, strongly depends on the quantity and quality of the available training data, often requiring large datasets to accurately capture complex system behaviors. When the training data are limited or exhibit distributional shifts, the performance of RC may degrade significantly, and the resulting model becomes difficult to interpret. In contrast, model driven approaches incorporate prior knowledge grounded in domain-specific physics, which reduces dependence on extensive data and improves both interpretability and generalization capability [29], [30], [31], [32]. For instance, Physics-Informed Neural Networks (PINN) is proposed for fiber transmission modeling by incorporating physical laws directly into the loss functions [33].

Inspired by the principle of TDRC and PINN, this paper introduces an LED model-driven RC equalizer for OFDM-VLC systems, in which the digitized physical model of the LED is integrated into the reservoir layer within the digital domain, thereby enabling explicit representation of LED characteristics, including low-pass response, static and dynamic nonlinearities, and memory effects, while avoiding the reliance on specialized photonic hardware required by photonic RC implementations. The main contributions of this work are as follows:

- We introduce a new RC framework that substitutes the conventional randomly-connected reservoir layer with a digitally implemented LED model. This model inherently captures the critical dynamics of the LED channel, including the low-pass response, nonlinearity, and memory effects, thereby enabling more precise signal equalization. By replacing physical nonlinear nodes with a digital counterpart, our approach not only reduces the hardware overhead associated with analog RC systems but also provides a more efficient and integrated solution for channel impairment compensation.

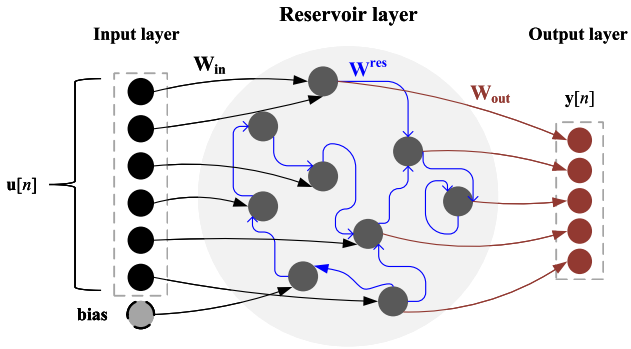

Fig. 1. Structure of the traditional RC.

- We propose frequency-domain regression for OFDM systems, where effective information is encoded in the frequency domain. This approach directly retrieves the signal in the frequency domain, whereas traditional time-domain regression requires additional steps to convert the signal into the frequency domain to extract the effective information.
- The proposed LED model-driven RC effectively reduces system BER, improves throughput, and exhibits strong generalization capability across diverse datasets. In comparison to Volterra, traditional RC and deep neural network (DNN) equalizer, it achieves significant performance improvements, particularly under challenging conditions such as limited training data and rapid channel variations. Experimental validation demonstrates the effectiveness of the algorithm, further confirming its practical applicability.

This paper is organized as follows. Section II introduces the proposed LED model-driven reservoir computing framework. In Section III, the proposed method is applied to OFDM-VLC systems and its performance is compared with conventional one-tap equalizer, Volterra equalizer, standard RC, and DNN approaches. Finally, Section IV concludes the paper.

II. LED Model-Driven RC

A. Traditional RC

The traditional RC network consists of three main components including the input layer, the reservoir layer, and the output layer, as illustrated in Fig. 1. The input layer receives the signal $\mathbf{u}[n]$ and feeds it into the reservoir layer, where nonlinear transformation is performed. The reservoir contains a large number of sparsely connected neurons, which together form a high-dimensional dynamic system. Nonlinearity is introduced through activation functions that enable the network to capture complex relationships and temporal dependencies. The output layer maps the reservoir layer output to the target. In RC, only the output weights are subject to training, typically through ridge regression. The internal weights remain fixed, which substantially reduces the computational burden and training time.

The reservoir state $\mathbf{s}[n]$ and the network output $\mathbf{y}[n]$ are updated using the following equations

$$\mathbf{s}[n+1] = (1-\alpha)\cdot\mathbf{s}[n] + \alpha$$

$$\cdot f\left(\mathbf{W}_{in}\cdot\mathbf{u}[n+1]+\mathbf{W}^{res}\cdot\mathbf{s}[n]\right), \quad (1)$$

$$\mathbf{y}[n+1]=f_{\text{out}}\left(\mathbf{W}_{out}\cdot[\mathbf{u}[n+1];\mathbf{s}[n+1]]\right). \quad (2)$$

The leaking rate α in (1) emulates exponential decay in the reservoir state, which aids in satisfying the echo state property and represents realistic physical implementations. $\mathbf{W}_{in}$ and $\mathbf{W}^{res}$ denote the input to reservoir and internal recurrent weight matrices, respectively. $\mathbf{u}[n]$ represent the input at time step n.

The training process involves recording reservoir states over time to construct the regression matrix $\mathbf{X}=[[1;\mathbf{s}[1];\mathbf{u}[1]],[1;\mathbf{s}[2];\mathbf{u}[2]],[1;\mathbf{s}[3];\mathbf{u}[3]],\dots]$, which incorporates the input signal, reservoir state, and a bias term. The corresponding target outputs are collected into the matrix $\mathbf{Y}_{\text{target}}$. The output weight matrix $\mathbf{W}_{\text{out}}$ is subsequently computed via ridge regression [34].

$$\mathbf{W}_{\text{out}}=\mathbf{Y}_{\text{target}}\cdot\mathbf{X}^T\left(\mathbf{X}\cdot\mathbf{X}^T+\zeta\mathbf{I}\right)^{-1}, \quad (3)$$

where ζ is a ridge regularization factor, used to ensure the stability and reliability of the enhanced RC, and $\mathbf{I}$ is the identity matrix. Here, $(\cdot)^T$ denotes the matrix transpose operation, and $(\cdot)^{-1}$ denotes the matrix inverse.

B. LED Nonlinear Model

LEDs are fundamental components in OFDM-VLC systems, where their nonlinear electro-optical characteristics, low-pass and memory effects significantly affect transmission performance. According to prior studies [35], the evolution of carrier concentration and the corresponding optical power emitted from an LED can be modeled by the following rate equations

$$\begin{cases}\frac{dn_c(t)}{dt}=\frac{I(t)}{qt_wA_w}-(B_rp_0+A_{nr})n_c(t)\\ \qquad -B_rn_c^2(t)-C_{nr}n_c^3(t),\\ P_{\text{opt}}(t)=\langle E_p\rangle A_wt_wB_r\left[p_0n_c(t)+n_c^2(t)\right],\end{cases} \quad (4)$$

where $n_c(t)$ denotes the electron concentration in the active region of the LED junction, while $P_{\text{opt}}(t)$ represents the corresponding optical power output. $I(t)$, q, t_w and A_w are the injected current, elementary charge, thickness, and area of the active layer, respectively. $\langle E_p\rangle$ is the average photon energy. A_{nr} and C_{nr} represent the Shockley–Read–Hall (SRH) and Auger recombination coefficients, respectively, and B_r is the bimolecular recombination constant. This model captures low-pass, nonlinearity, and memory effect, which are crucial for accurately describing the signal distortion in LED channels.

The nonlinear dynamics of LEDs can be discretized from the rate equations in (4). The resulting approximation is expressed as

$$\begin{cases}n_c(t+T_s)\approx n_c(t)+T_s\dfrac{dn_c(t)}{dt}\\ \approx a_0I(t)+a_1n_c(t)+a_2n_c^2(t)+a_3n_c^3(t),\\ P_{\text{opt}}(t+T_s)=a_4n_c(t+T_s)+a_5n_c^2(t+T_s),\end{cases} \quad (5)$$

where T_s is the sampling interval, and the parameters a_0 to a_5, which define the intrinsic physical properties of the LED, are closely related to its material composition, manufacturing process, and operating environment. Specifically, $a_0=T_s/(qt_wA_w)$, $a_1=1-B_rp_0T_s-A_{nr}T_s$, $a_2=-B_rT_s$, $a_3=-C_{nr}T_s$, $a_4=\langle E_p\rangle A_wt_wB_rp_0$, and $a_5=\langle E_p\rangle A_wt_wB_r$.

The output power is primarily determined by the linear term $a_4n_c(t+T_s)$ under low levels of injected current. As the injected current increases, the nonlinear term $a_5n_c^2(t+T_s)$ becomes more prominent, leading to noticeable signal distortion.

The LED equations in (4) and (5) inherently encapsulate the critical impairments of the LEDs, i.e., low-pass filtering, nonlinear distortion, and memory effects. By explicitly accounting for these phenomena, the model thus offers a holistic and accurate description of the entire VLC link, thereby serving as a reliable foundation for system modelling and impairment compensation.

C. LED Model-Driven RC

The framework for the LED model-driven RC retains the standard three-layer architecture of reservoir computing, comprising an input layer, a reservoir layer, and an output layer, as illustrated in Fig. 2(a). The key architectural difference lies in replacing the conventional randomly connected neural reservoir with a digitized nonlinear physical model derived from the LED.

The proposed model-driven RC leverages the nonlinearity and fading memory characteristics of the LED, as presented in Fig. 2(b). The current output is influenced by previous inputs through feedback coefficients a_1, a_2 and a_3. Meanwhile, the nonlinear term with a_5 enables effective projection of the input signal into a high-dimensional state space. These nonlinearity and fading memory properties make the LED model well-suited for implementing RC. Furthermore, the series data processing in (5) inherently implements an LED-based TDRC, where the virtual nodes in the reservoir are driven by a time-multiplexed, serialized input signal [36].

In the input layer, the received serial signal is first normalized to mitigate amplitude fluctuations induced by channel impairments, thereby enhancing the robustness of subsequent processing. The normalized signal is then converted from serial to parallel, forming the OFDM signal matrix $\bar{\mathbf{X}}=[\bar{\mathbf{x}}_1,\dots,\bar{\mathbf{x}}_L]\in\mathbb{R}^{(N_{\text{fft}}+CP)\times L}$, where each column $\bar{\mathbf{x}}_n\in\mathbb{R}^{(N_{\text{fft}}+CP)\times 1}$ (with $n=1,2,\dots,L$) represents an individual OFDM symbol, and L denotes the total number of OFDM symbols used for training. Here, N_{fft} denotes the fast Fourier transform (FFT) size, and CP refers to the Cyclic Prefix (CP) length.

The reservoir layer is digitally implemented using a time multiplexed structure consisting of N virtual nodes. To ensure alignment with these nodes, each input symbol $\bar{\mathbf{x}}_n$ is upsampled by the factor N, resulting in an expanded vector $\bar{\mathbf{u}}_n\in\mathbb{R}^{((N_{\text{fft}}+CP)\cdot N)\times 1}$. This upsampled vector $\bar{\mathbf{u}}_n$ is then fed into the reservoir layer as the input sequence. The inclusion of a CP enhances the ability of the reservoir to capture ISI and channel impairments. The reservoir state $\bar{\mathbf{s}}[i]$ represents a numerical abstraction of the carrier concentration dynamics in the LED junction, while the output $\bar{\mathbf{y}}[i]$ corresponds to the modeled electro-optical response. Their system dynamics are governed by

$$\begin{cases}\bar{\mathbf{s}}[i+1]=a_0\bar{\mathbf{u}}[i]+a_1\bar{\mathbf{s}}[i]+a_2\bar{\mathbf{s}}[i]^2,\\ \bar{\mathbf{y}}[i+1]=a_4\bar{\mathbf{s}}[i+1]+a_5\bar{\mathbf{s}}[i+1]^2,\end{cases} \quad (6)$$

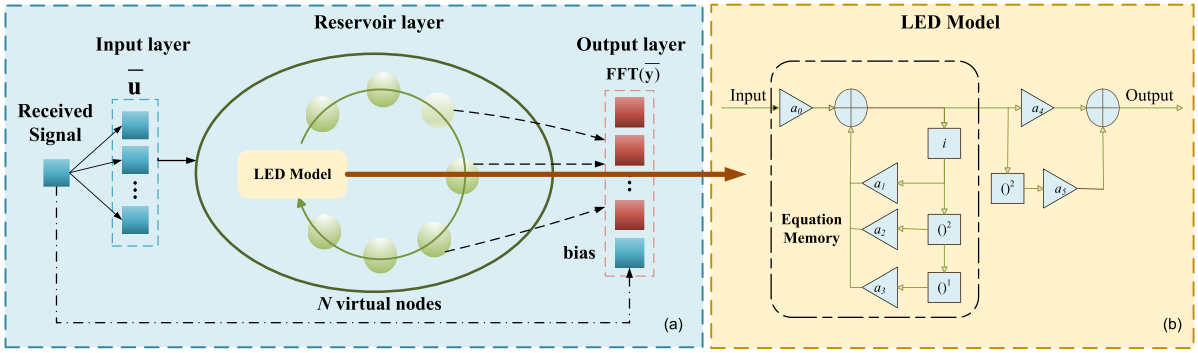

Fig. 2. (a) Structure of the model-driven RC. (b) Time-discretized LED nonlinear model.

where the index i denotes the discrete time step in the sequential processing of the upsampled input vector. The resulting sequence $\bar{\mathbf{y}}_n[i]$ encapsulates the complete temporal response of the reservoir to the n-th symbol. All output vectors are then stacked to form the reservoir output matrix $\bar{\mathbf{Y}} = [\bar{\mathbf{y}}_1, \ldots, \bar{\mathbf{y}}_L]$.

The RC framework is adapted to align with the characteristics of OFDM-VLC systems by extending traditional time-domain linear regression into the frequency domain. This transformation compensates for frequency-selective distortions introduced by the LED, removes Hermitian symmetric subcarriers to eliminate redundancy, and facilitates independent equalization across effective subcarriers. This design is based on the inherent structure of OFDM signals, where information is carried by orthogonal subcarriers and channel impairments manifest primarily as frequency-domain effects. Operating directly on the demodulated subcarriers allows the regression to focus on the effective information components rather than redundant time-domain samples. This enables efficient regression.

Therefore, in the output layer, the FFT is applied to both the reservoir output matrix $\bar{\mathbf{Y}}$ and the corresponding OFDM signal matrix $\bar{\mathbf{X}}$. After removing the CP, the Hermitian symmetric subcarriers are discarded, and only the effective subcarriers are retained, resulting in the final frequency domain representations $\bar{\mathbf{Y}}'$ and $\bar{\mathbf{X}}'$. The matrices $\bar{\mathbf{X}}'$ and $\bar{\mathbf{Y}}'$ are concatenated to form $\mathbf{Z} = [\bar{\mathbf{X}}'; \bar{\mathbf{Y}}']$. The resulting matrix is then reshaped to obtain the regression matrix $\mathbf{Z}_1 \in \mathbb{C}^{(N+1)\times(N_{sub}\times L)}$, where N_{sub} denotes the number of effective subcarriers. Each column comprises the dynamic response extracted from the reservoir and a bias term computed from the received signal. The output weights of the network are then calculated using ridge regression

$$\bar{\mathbf{W}}_{\text{out}} = \bar{\mathbf{Y}}_{\text{target}} \cdot \mathbf{Z}_1^T \cdot \left(\mathbf{Z}_1 \cdot \mathbf{Z}_1^T + \zeta \mathbf{I}\right)^{-1}. \tag{7}$$

In (7) ζ is the regularization coefficient and $\bar{\mathbf{Y}}_{\text{target}}$ denotes the target frequency-domain training matrix. In the test stage, the equalized signal is computed using

$$\bar{\mathbf{Y}}_{out} = \bar{\mathbf{W}}_{out} \cdot \mathbf{Z}_2, \tag{8}$$

where $\mathbf{Z}_2$ is the matrix obtained by processing the testdata in the same steps as the $\mathbf{Z}_1$.The detailed procedure of the model-driven algorithm is outlined in Algorithm 1.

Algorithm 1: Model-Driven RC Equalization.

Given: Received serial signal and virtual nodes number N.

Phase 1 – Data Preprocessing and Initialization

- Normalized signal and converted from serial to parallel to obatan matrix $\bar{\mathbf{X}} = [\bar{\mathbf{x}}_1, \ldots, \bar{\mathbf{x}}_L] \in \mathbb{R}^{(N_{fft}+CP)\times L}$.

Phase 2 – Nonlinear Feature Extraction by LED Modeling

- **Input:** OFDM signal matrix $\bar{\mathbf{X}}$.
- **For each column vector $\bar{\mathbf{x}}$ in $\bar{\mathbf{X}}$:**
  - Initialize reservoir state: $\bar{s}(0) = 0$.
  - Upsampled by the factor N to obtain $\bar{\mathbf{u}}_n$.
  - **For each scalar element in $\bar{\mathbf{u}}$:**
    - Compute the reservoir state and response using the LED model equations (6).
- Collect all outputs to form the output matrix $\bar{\mathbf{Y}}$
- Apply cyclic prefix removal, FFT, and De-Hermitian transformations to both $\bar{\mathbf{Y}}$ and $\bar{\mathbf{X}}$ to obtain their frequency-domain representations $\bar{\mathbf{Y}}'$ and $\bar{\mathbf{X}}'$.

Phase 3 – Output Regression

- Concatenate $\bar{\mathbf{X}}'$ (as bias) and $\bar{\mathbf{Y}}'$ to obtain the $\mathbf{Z}$, and then reshape $\mathbf{Z}$ to form the final regression matrix $\mathbf{Z_1}$.
- Compute the output weight matrix $\bar{\mathbf{W}}_{\text{out}}$ using a regression by (7).

Phase 4 - Testing

- Compute the corresponding outputs using (8) with the learned weights $\bar{\mathbf{W}}_{\text{out}}$ for the testing data.
- Evaluate the performance of the model-driven RC.

III. Experiment Results and Discussions

The proposed model-driven RC equalization method is experimentally verified in an OFDM-VLC system. The system architecture is shown in Fig. 3(a). In this study, random bit sequences derived from atmospheric noise are used to generate the signal, avoiding performance overestimation. At the transmitter, the random bit stream is first mapped to M-QAM symbols and then converted from Serial to Parallel (S/P) for OFDM modulation. Hermitian symmetry is applied to the frequency-domain data to produce a real-valued time-domain waveform after the Inverse Fast Fourier Transform (IFFT). After CP insertion, parallel-to-serial (P/S) conversion is applied for further Digital to Analog

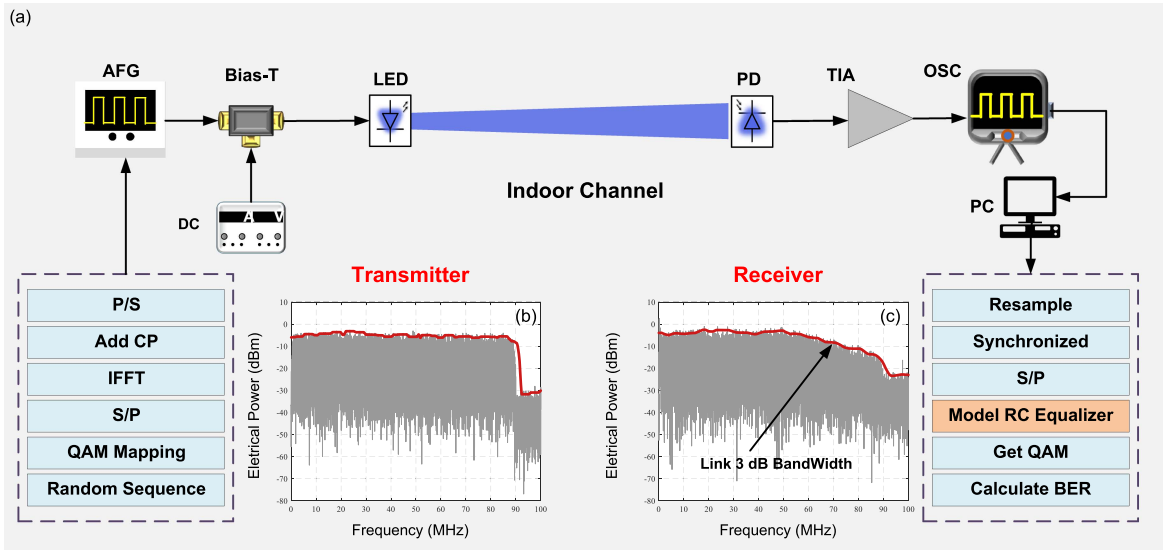

Fig. 3. System architecture and spectral characteristics of the OFDM-VLC transmission link. (a) Experimental diagram of OFDM-VLC system. (b) Power spectrum of the transmitted OFDM signal in grey and its envelope in red, (c) power spectrum of the received OFDM signal in grey and its envelope in red.

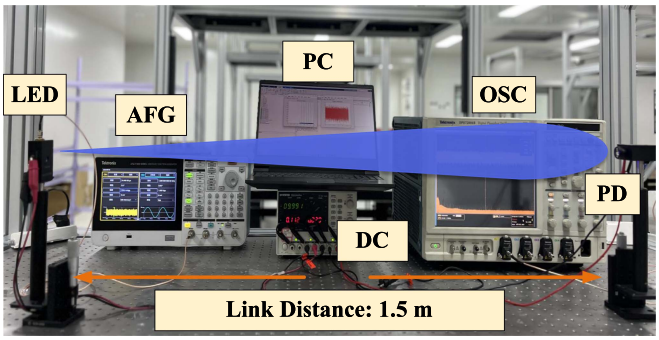

Fig. 4. Experimental setup of the OFDM-VLC system.

Conversion (DAC) in an Arbitrary Function Generator (AFG). The LED is driven by the modulated analog signal combined with a DC bias to enable proper optical modulation.

At the receiver, the incident optical signal is focused onto a photodetector. The converted electrical waveform is subsequently digitized by an oscilloscope. Offline Digital Signal Processing (DSP) comprising signal resampling, model-driven RC equalization, OFDM demodulation is applied to obtain the BER. The experimental setup is shown in Fig. 4, with the key system parameters summarized in Table I. Fig. 3(b) and (c) show the power spectra of a 90 MHz OFDM signal at the transmitter and receiver, respectively. From these transmitted and received spectra, the frequency response of the link is estimated by the envelope, yielding an approximate 3 dB bandwidth of 70 MHz. This low-pass characteristic is mainly attributed to the LED, which dominates the frequency response of the optical wireless link.

In the experiment, the OFDM-VLC link operates over a communication distance of approximately 1.5 meters. This setup simulates a typical short-range indoor optical wireless communication scenario, providing a realistic evaluation of the performance under operational conditions.

TABLE I
EXPERIMENT PARAMETERS FOR THE OFDM-VLC SYSTEM

Parameters	Experiment
FFT/IFFT Size	128
Number of data-carrying subcarriers	63
QAM signal modulation order	16QAM, 32 QAM
Length of cyclic prefix	8
Signal Bandwidth	30, 40, 50, 60, 70, 80, 90 MHz
DC Bias	10 V
LED 3-dB Bandwidth	70 MHz
Photodetector 3-dB Bandwidth	230 MHz
Communication Distance	1.5 m
DAC sampling rate	1 GSa/s, 2 GSa/s
ADC sampling rate	6.25 GSa/s
LED wavelength	459.3 nm
Traditional RC hidden units	35
Model-driven RC hidden units	6
RC ridge regularization factor	10^{-8}
Number of training/testing symbols	120, 1080

A. Parameters Estimation and Equalizers Configuration

1) Parameters Estimation for LED Model-Driven RC: The estimation of LED model parameters a_0 to a_5 is inherently influenced by the DAC sampling rate, as it determines the temporal resolution at which the nonlinear behavior is captured. To evaluate the robustness of the proposed model-driven RC equalization under different sampling conditions, parameter sets are extracted at sampling rates of 1 GSa/s and 2 GSa/s. These sampling rates are chosen to assess the impact of temporal resolution on parameter estimation and the resulting model

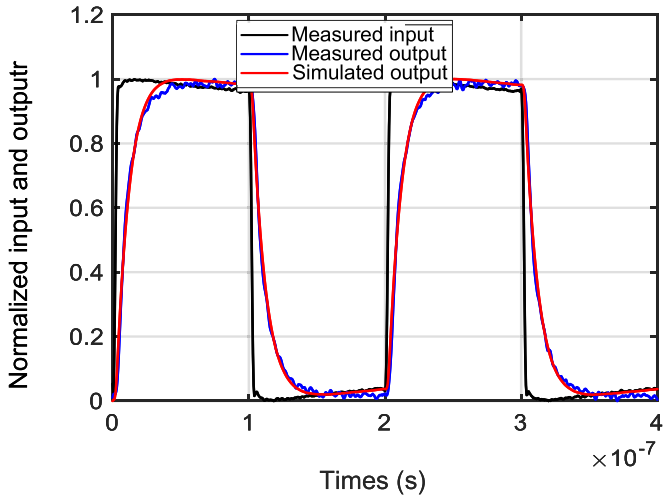

Fig. 5. Measured and simulated LED output with nonlinearity, using a square waveform of 5 MHz with 2 GSa/s sampling rate.

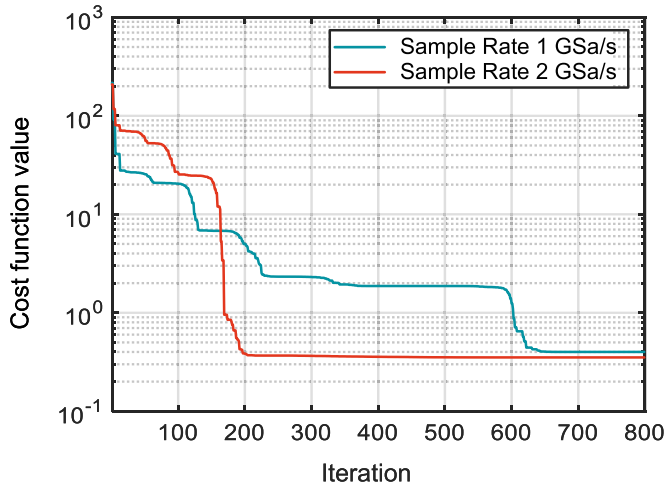

Fig. 6. Cost function values and iterations for LED parameters estimation by 5 MHz square wave with different sampling rate.

performance. The Least Mean Squares (LMS) algorithm is used for parameter estimation during the training process, which is further detailed in a previous study [35].

For clarity, a representative parameter estimation setting at a sampling rate of 2 GSa/s is provided. A 5 MHz square-wave signal with a modulation voltage of 200 mV is applied, and 1200 sampling points corresponding to two complete periods are collected. These input and output samples are used to estimate the LED model parameters. Fig. 5 compares the original square wave with the measured waveform after modulation by the LED. The measured rise time is 85 ns, while the fall time is 105 ns, reflecting the dynamic behavior of the LED influenced by nonlinear and memory effects described by the rate equations. Meanwhile, the simulated waveform generated by the nonlinear LED model closely matches the waveform modulated by the LED, confirming that the LED model parameters are accurately extracted and enable precise representation of the LED nonlinear behavior. Since the model explicitly incorporates low-pass characteristics, memory effects, and both static and dynamic nonlinearities, variations under different operating conditions can be accommodated through parameter recalibration within the same model structure.

Fig. 6 shows the cost function during the training process. The cost value gradually decreases and converges as the number of iterations increases, demonstrating the effectiveness of the parameter estimation process. The parameter estimation with 1 GSa/s was performed using the same methodology with 2 GSa/s. A summary of the estimated parameters is provided in Table II, where the values of a_0 to a_5 for both the 1 GSa/s and 2 GSa/s sampling rates are listed. While the estimated parameters are different due to parameters are inherently influenced by the sampling rate [35], both sets of parameters can be utilized in the proposed RC model, as well as the LED behavior is accurately represented.

2) Equalizers Configuration and Optimization: The performance of the proposed model-driven RC algorithm is evaluated against the one-tap, Volterra, and traditional RC algorithms.

TABLE II
ESTIMATED PARAMETERS FOR THE LED MODEL (NORMALIZED)

Parameters	Estimated values at 1 GSa/s	Estimated values at 2 GSa/s
$a_0 \times 10^{15}$	33.479	40.657
a_1	0.988	0.988
$a_2 \times 10^{-21}$	-7.932	-6.484
a_3	0	0
$a_4 \times 10^{-19}$	2.961	4.397
$a_5 \times 10^{-35}$	0.283	-0.351

The one-tap equalizer serves as a linear reference, whereas the Volterra and traditional RC algorithms serve as nonlinear benchmarks. All methods are trained and tested on the same dataset, which consists of 120 OFDM symbols for training and 1080 symbols for testing. Parameters of the Volterra, traditional RC, and model-driven RC algorithms are optimized within the OFDM-VLC system under identical conditions to ensure fair comparison.

In VLC systems, each equalizer requires a distinct set of optimal parameters for different modulation orders and channel conditions, particularly for the Volterra and traditional RC equalizers. The optimization process remains fundamentally consistent across varying system configurations. In this study, the 16 QAM modulation format with a 40 MHz signal bandwidth is selected as an example to illustrate the optimization process.

The Volterra equalizer is implemented as a second-order nonlinear filter, as prior studies have shown that second-order Volterra models are sufficient to capture the dominant nonlinearities in VLC systems [37], and the adopted Volterra structure is further optimized through kernel symmetry to reduce redundant coefficients. Fig. 7 presents the convergence behavior of the Volterra parameters, which is evaluated using the cost function defined as

$$e(n) = \frac{1}{N'} \sum_{1}^{N'} \left[\hat{y}(n) - y_{\text{ref}}(n)\right]^2, \tag{9}$$

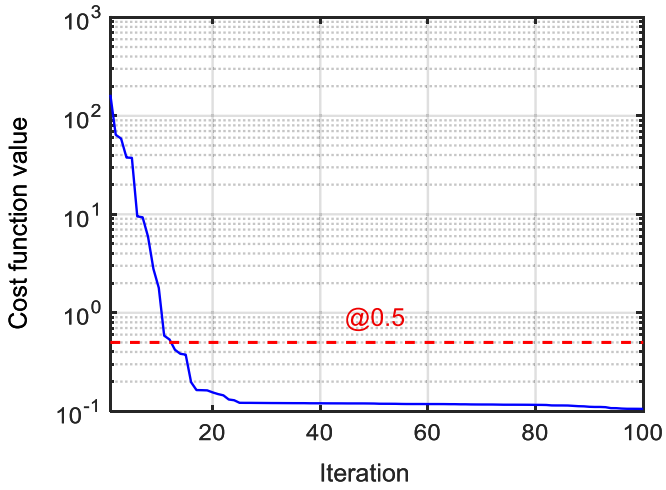

Fig. 7. Cost function values and iterations for Volterra equalizer parameter estimation in 16 QAM OFDM-VLC system.

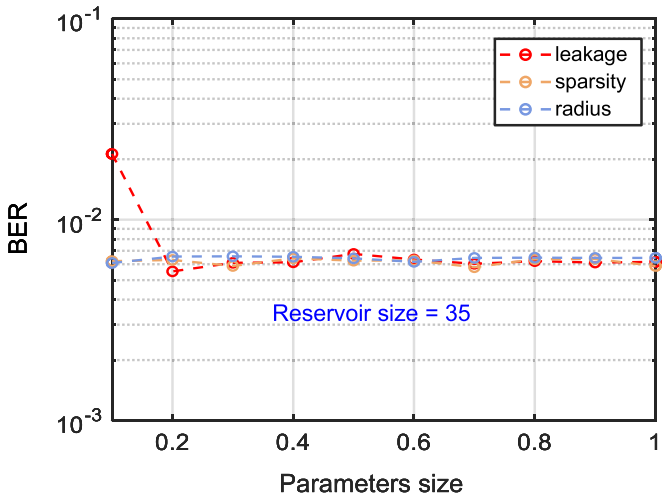

Fig. 9. BER performance with varying hyperparameter values for traditional RC in 16 QAM OFDM-VLC system.

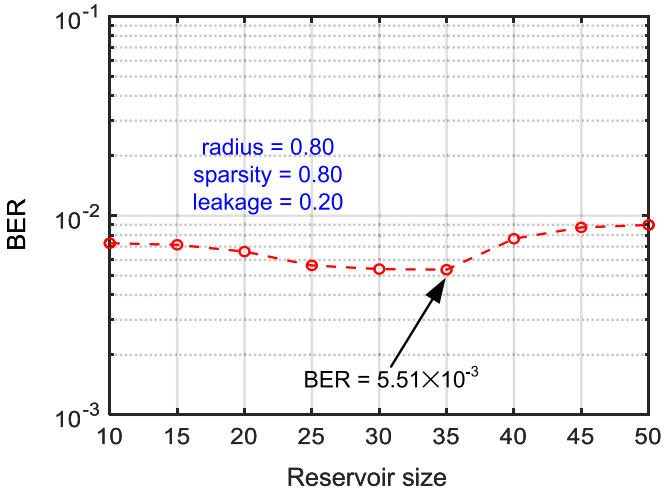

Fig. 8. BER performance with varying reservoir size for traditional RC in 16 QAM OFDM-VLC system.

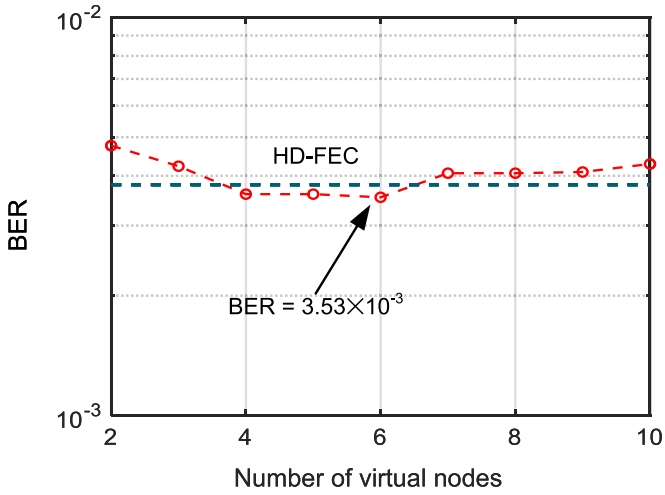

Fig. 10. Effect of the number of virtual nodes on the BER performance of model-driven RC in 16 QAM OFDM-VLC system.

where $\hat{y}(n)$ denotes the equalizer output, $y_{\text{ref}}(n)$ is the reference signal, and N' represents the number of reference samples. The cost function converges and stabilizes below 0.5 after approximately 20 iterations, followed with a stable and optimal configuration.

The traditional RC equalizer hyperparameters are also examined to ensure a fair performance comparison with the Volterra and model-driven equalizer. Key architectural parameters, including the reservoir size, leakage rate, sparsity, and spectral radius, are evaluated in Figs. 8 and 9. As shown in the previous study, when evaluating the impact of a single parameter, the other hyperparameters are fixed at their default values [38]. The optimal BER performance is achieved with a reservoir size of approximately 35, a leakage rate of 0.20, sparsity of 0.80, and a spectral radius of 0.80. These results demonstrate the significant influence of each parameter on the system performance, and emphasize the importance of selecting appropriate values to optimize the traditional RC equalizer performance.

In contrast, the LED model-driven RC approach requires no tuning of conventional hyperparameters. After the physical parameters of the LED model are determined, the internal reservoir dynamics are fully specified, leaving the number of virtual nodes as the only adjustable structural parameter. By varying the number of virtual nodes, the model enhances its nonlinear mapping capability without introducing additional hyperparameter optimization [39]. Fig. 10 illustrates the effect of the number of virtual nodes on the performance of the model-driven RC. The minimum BER is achieved with 4 to 6 virtual nodes, while using more than six nodes may introduce redundant information, potentially degrading system performance.

For completeness, a lightweight DNN equalizer is also considered as a data-driven reference for comparison. To ensure a fair and controlled evaluation, the adopted DNN employs a compact architecture composed solely of fully connected layers with lightweight nonlinear activation functions. This intentionally constrained structure represents the simplest neural network

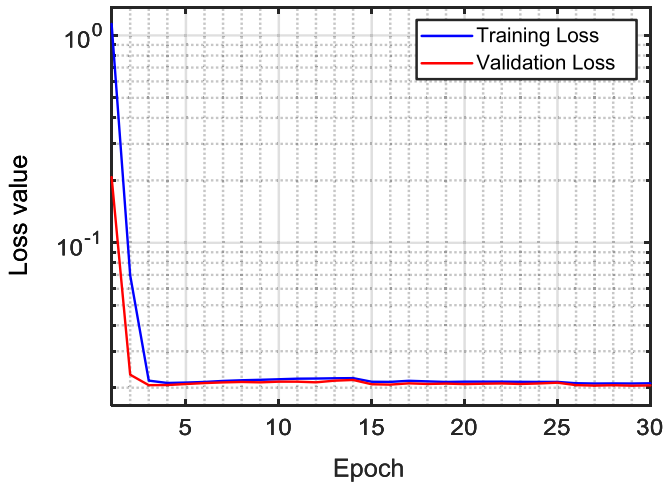

Fig. 11. Train and validation loss of the DNN during the gradient descent optimization process in 16 QAM OFDM-VLC system.

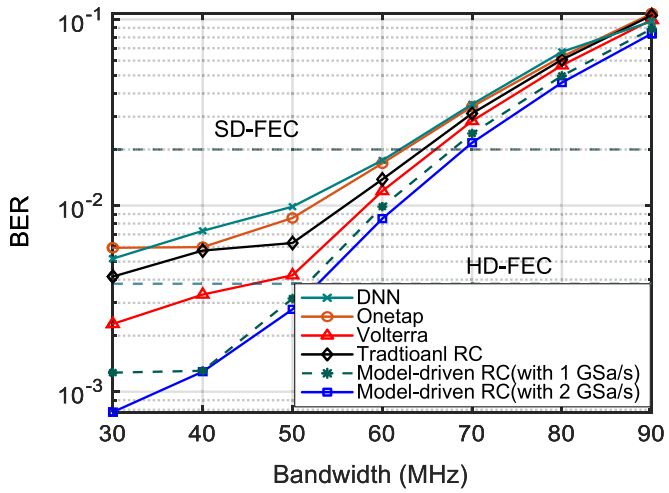

Fig. 12. BER performance of different equalization algorithms for 16 QAM modulation under varying bandwidth conditions.

capable of nonlinear mapping, while avoiding excessive model capacity or complex architectural components. The network is trained using the mean squared error (MSE) as the loss function, and the model parameters are optimized by gradient descent. As a result, the comparison emphasizes intrinsic modelling characteristics rather than advantages arising from overparameterization. The evolution of the training loss and the validation loss during the optimization process is illustrated in Fig. 11, which shows the convergence behavior of the model over 30 training epochs.

B. Equalization Performance Evaluation and Comparison

1) Performance With Varying Bandwidth: The BER performance of the proposed model-driven RC algorithm is compared with the one-tap, Volterra, traditional RC and DNN equalizers. Fig. 12 presents the BER of 16 QAM signals as the signal bandwidth varies from 30 MHz to 90 MHz, under a modulation voltage of 200 mV. As the modulation bandwidth increases, the low pass characteristic of the channel becomes more pronounced, leading to significant attenuation of high-frequency components. Additionally, the inherent nonlinear and memory effects of the LED, result in a consequent increase in the BER for the 16 QAM system.

Over the full bandwidth range, the one-tap equalizer can only recover linear distortions, whereas the model-driven RC algorithm more efficiently compensates for low-pass and nonlinear effects, resulting in superior signal recovery. The DNN equalizer exhibits BER performance comparable to that of the one-tap equalizer, indicating limited capability in mitigating low-pass effects and both static and dynamic nonlinear distortions under the considered bandwidth conditions. This advantage is particularly evident at a signal bandwidth of 50 MHz, where the model-driven RC achieves a BER of 2.76×10^{-3}, compared to 4.22×10^{-3} for Volterra and 6.28×10^{-3} for traditional RC. At this condition, the model-driven RC achieves a 34.6% and 56.0% reduction in BER compared to traditional RC and Volterra, respectively, and only the model-driven RC maintains the HD-FEC error threshold under challenging channel conditions.

The achievable rate R of the OFDM-VLC system is calculated by

$$R = \Delta f \sum_{k=1}^{K} \log_2\left(1 + \frac{SNR_k}{\Gamma}\right), \tag{10}$$

where Γ is the modulation gap derived from the BER performance [40], SNR_k denotes the SNR of the k-th subcarrier, K is the total number of subcarriers, and Δf is the subcarrier spacing. The signal-to-noise ratio for each subcarrier is calculated from the Error Vector Magnitude (EVM), defined as

$$\begin{cases} \mathrm{EVM}_k = \sqrt{\dfrac{\sum_{i=1}^{N} \left|\hat{s}_{i,k} - s_{i,k}\right|^2}{\sum_{i=1}^{N} \left|s_{i,k}\right|^2}}, \\ \mathrm{SNR}_{k,\mathrm{dB}} = -20\log_{10}(\mathrm{EVM}_k), \end{cases} \tag{11}$$

where $\hat{s}_{i,k}$ and $s_{i,k}$ represent the equalized received constellation symbols and the transmitted constellation symbols of the k-th subcarrier, respectively.

Fig. 13 illustrates the achievable rate of the system with various equalizers. The achievable rate increases with bandwidth from 30 MHz to 70 MHz. However, when the bandwidth exceeds 70 MHz, the achievable rate begins to decrease. This behavior is expected because the system approaches its 3 dB bandwidth limit around 70 MHz, as shown in Fig. 3(b) and (c). Further increasing the bandwidth shifts more subcarriers into the higher-loss region above 70 MHz, leading to performance degradation. This observation is consistent with our previous findings [41]. Consistent with the BER results, the achievable rate of the DNN equalizer remains similar to the one-tap equalizer over the entire bandwidth range. At 70 MHz, the achievable rate of the model-driven RC algorithm reaches 247.44 Mbps, approximately 13% higher than the 219.50 Mbps of traditional RC and 10% higher than the 226.42 Mbps of the Volterra algorithm in the 16 QAM OFDM-VLC system.

Moreover, to assess the impact of sampling rate on the model-driven RC algorithm, performance comparisons were conducted using two different sampling rates, 1 GSa/s and 2 GSa/s. Applied

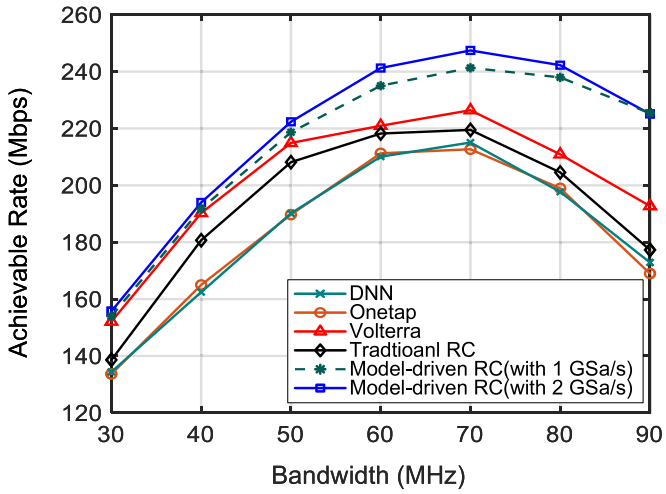

Fig. 13. Achievable rate of different equalization algorithms for 16 QAM modulation under varying bandwidth conditions.

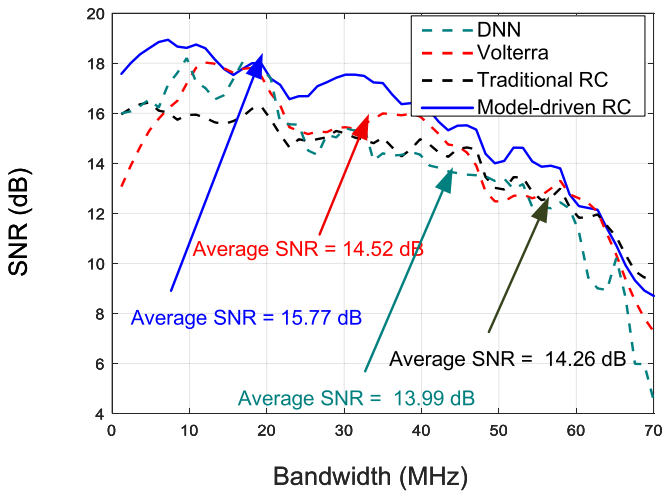

Fig. 14. SNR performance of each subcarrier in 16 QAM OFDM-VLC system for different equalization algorithms.

with different estimated parameters from a_0 to a_5 in Table II, Figs. 12 and 13 show that the proposed algorithm maintains stable performance in terms of BER and achievable rate across the entire bandwidth range. These results reveal that the model-driven RC algorithm exhibits high robustness various sampling conditions. For all subsequent experiments in this study, the parameters estimated with a 2 GSa/s sampling rate were used.

Fig. 14 further presents the per-subcarrier SNR of the 16 QAM OFDM-VLC system at a 70 MHz bandwidth. At this bandwidth, the system achieves its maximum throughput, as shown in Fig. 13. The model-driven RC algorithm consistently yields a higher average SNR across all subcarriers compared with both the Volterra and traditional RC equalizers. In contrast, the DNN equalizer achieves a lower average SNR of 13.99 dB, which is approximately 2 dB lower than that obtained by the model-driven RC approach. The average SNRs are 15.77 dB for the model-driven RC, 14.52 dB for the Volterra equalizer, and 14.26 dB for traditional RC. In the lower-frequency region, particularly below 60 MHz, the channel exhibits a relatively higher SNR, allowing the model-driven RC algorithm to maintain better per-subcarrier SNR and signal integrity. However, as the bandwidth increases and the signal extends into higher frequencies, system performance degrades due to the intrinsic bandwidth limitation of the LED.

Since the DNN equalizer exhibits performance comparable to that of the one-tap equalizer, subsequent performance evaluations focus on the remaining nonlinear equalization schemes. The computational complexity of the DNN equalizer is nevertheless included for completeness.

2) Performance With Varying Modulation Voltage: The performance of the proposed algorithm is evaluated under varying SNR conditions by adjusting the modulation peak-to-peak voltage from 100 mV to 240 mV, while maintaining a fixed signal bandwidth of 40 MHz. This bandwidth configuration ensures a relatively flat system frequency response, thereby minimizing the low-pass characteristics of the LED and enabling a more accurate assessment of the capability to compensate for nonlinear signal distortion.

For each modulation voltage, the BER is calculated by averaging the results of 10 independent experiments, in which the complete transmission, equalization, and BER evaluation processes are independently repeated. To further assess the statistical reliability of the results, 95% confidence intervals are calculated and plotted based on these experimental results. Considering the limited number of independent experiments and the unknown population variance, the confidence intervals are estimated using the t-distribution with 9 degrees of freedom, which is appropriate for small-sample statistical inference. As illustrated in Fig. 15(a), increasing the modulation voltage results in a more pronounced reduction in BER for the proposed model-driven RC approach, which consistently outperforms the Volterra-based and traditional RC algorithms over the considered voltage range.

Fig. 15(b) shows the received signal constellation, where the nonlinear distortions are evident. As the modulation voltage increases, the nonlinearity of the LED intensifies, further distorting the received signal. Fig. 15(c), (d), and (f) present the constellation diagrams for the three equalizer algorithms at the corresponding modulation voltages. Fig. 15(c) shows clearer signal constellations compared to the other methods, which demonstrates the superior capability of the model-driven RC in restoring signal nonlinear distortion.

C. Generalization Capability Analysis

1) Effect of SNR Mismatch: SNR mismatch conditions are introduced to evaluate the robustness and stability of the proposed model-driven RC under different noise conditions between the training and testing stages. The model is trained using data collected at a modulation voltage of 240 mV, corresponding to an estimated receiver SNR of approximately 18.2 dB, and evaluated using data collected at a modulation voltage of 200 mV, corresponding to an estimated receiver SNR of approximately 16.5 dB. The receiver SNR values are estimated from the received and transmitted constellation points using (11). This

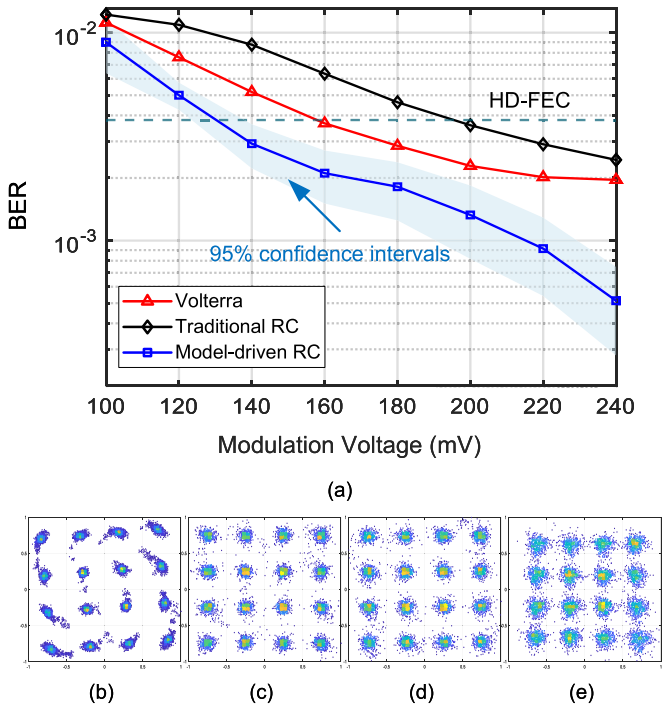

Fig. 15. (a) BER performance and 95% confidence intervals of 16 QAM OFDM-VLC system with different modulation voltage. Constellation diagrams of received signal (b) and after the model-driven RC (c), Volterra (d), and traditional RC (e) equalization at a modulation voltage of 240 mV.

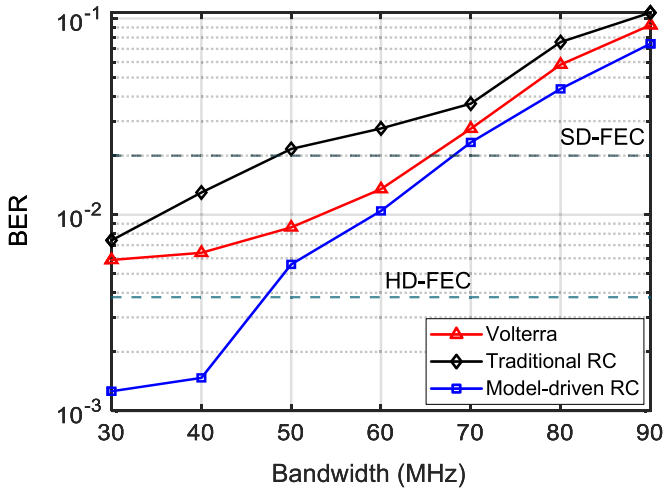

Fig. 16. BER performance across different bandwidths for model-driven RC, Volterra, and traditional RC under SNR mismatch conditions.

configuration represents a moderate degradation of the channel quality between the training and testing conditions.

Fig. 16 shows the BER performance of various equalizers under 16 QAM OFDM modulation. To ensure fairness, the ratio between training and testing data remains constant during optimization for all equalizers. Compared with the results under matching SNR conditions in Fig. 12, performance degradation is observed for all equalizers due to the SNR mismatch between training and testing conditions. Despite this, the model-driven RC consistently outperforms both Volterra and traditional RC equalizers, achieving a lower BER across all signal bandwidths.

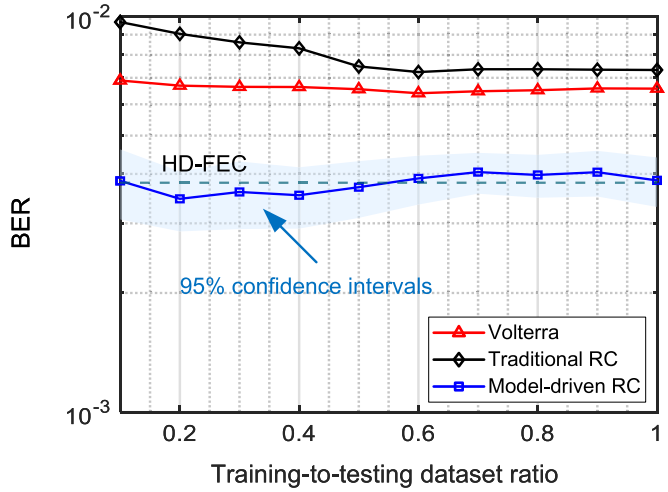

Fig. 17. BER performance under varying training sample size at 40 MHz for Volterra, traditional RC and model-driven RC equalizer with 95% confidence intervals.

2) Effect of Training Size: The effect of training sample size on equalization performance was evaluated by fixing the test dataset to 1080 OFDM symbols, while the number of training samples was gradually increased and expressed as a percentage relative to the fixed test set size. All experiments were conducted at a signal bandwidth of 40 MHz, where the channel frequency response remains relatively flat and low pass distortion is moderate. This bandwidth setting allows the impact of the training sample size on equalization performance to be clearly observed without being dominated by severe bandwidth limitations. To further examine the learning capability of the equalizers, a higher-order modulation format such as 32 QAM was considered, as it is more sensitive to nonlinearity and equalization accuracy than 16 QAM.

Fig. 17 shows the BER performance for 32 QAM signals at 40 MHz with varying training data proportions. The BER results are averaged over multiple independent experiments, with the corresponding 95% confidence intervals, computed using the t-distribution due to the limited number of experiments, included to characterize performance variability. The model-driven RC approach achieves reliable BER performance with only 20% of the training data (216 symbols), with the confidence interval remaining mostly below the HD-FEC threshold. In contrast, the Volterra-based and traditional RC approaches require approximately 50% (540 symbols) of the training data, yet their confidence intervals are largely above the HD-FEC limit, indicating limited robustness under these conditions.

D. Computational Complexity Analysis

The first component of the computational cost arises from the per-sample signal processing and state update operations performed by each equalizer. For the one-tap equalizer, this operation is straightforward, as it involves only a single received sample and an FFT operation to transform the signal into the frequency domain. For the traditional RC, this operation requires updating the reservoir states through recurrent matrix–vector

multiplications, resulting in a per-sample computational complexity on the order of $O(N_r^2)$ to update N_r reservoir features, as directly implied by the state update in (1).

For the Volterra equalizer, the computational cost arises from the evaluation of nonlinear polynomial basis terms. The total number of terms for a p-th order equalizer with memory length M given by $\sum_{i=1}^{p}\binom{M+i-1}{i}$, where the binomial coefficient $\binom{M+i-1}{i}$ counts the number of distinct i-th order monomial terms. This formulation accounts for the structure of the Volterra kernels and provides a more accurate estimate of the number of coefficients, which is substantially lower than the naive upper bound of M^p. Nevertheless, despite being lower than the upper bound, the number of coefficients grows asymptotically as M^p. Moreover,the evaluation of these Volterra basis terms requires the corresponding multiplicative operations, and the number of such operations increases with the number of coefficients. Therefore, the feature generation complexity of the Volterra equalizer can be conservatively characterized as $O(M^p)$.

For the proposed model-driven RC, the per-sample computation is realized through a scalar LED-based recursion at each virtual node. According to the discrete LED model in (6), updating the state of a single virtual node involves a fixed number of arithmetic operations, resulting in an approximately constant computational cost per node. Therefore, updating the states of N_v virtual nodes leads to a per-sample complexity that scales linearly with with N_v. In addition, the model-driven RC performs regression in the frequency domain, which requires transforming the virtual node outputs by fast Fourier transforms, introducing an additional computational cost that scales as $O(N_v \log_2(N_v))$.

For consistency and fair comparison, implementation-dependent constant factors are omitted for all equalization schemes in the asymptotic complexity analysis, as these constants for the traditional RC and the Volterra equalizer depend on specific reservoir realizations and kernel constructions. Accordingly, the feature generation complexity of the proposed model-driven RC is expressed in a normalized form as $O(N_v \log_2(N_v) + N_v)$, while the other methods are characterized by their dominant scaling behaviors.

Based on the analysis above, the training complexity of the considered equalizers is evaluated under a closed-form least-squares (LS) regression framework like (3). Since all methods estimate their readout weights through closed-form LS solutions, the training complexity is dominated by matrix multiplications and matrix inversion operations inherent to the LS formulation. In this context, implementation-dependent constant factors are not introduced, and the complexity is characterized solely by the scaling behavior with respect to the feature dimension and the number of training samples.

For the traditional RC, the feature dimension D equals the reservoir size N_r. Given T training samples, the readout weights $\mathbf{W}_{\text{out}}$ are computed using (3), which involves matrix multiplication with a computational complexity of $O(TN_r^2)$ and matrix inversion requiring $O(N_r^3)$ operations. Therefore, the overall training complexity is dominated by $O(TN_r^2 + N_r^3)$.

For the Volterra equalizer, the feature dimension D is determined by the number of Volterra coefficients. For complexity benchmarking, the asymptotic upper bound $D = M^p$ is adopted for a p-th order equalizer with memory length M. Under the closed-form LS training framework, constructing the regression matrices requires$O(TM^{2p})$ operations, while solving the resulting linear system incurs an additional $O(M^{3p})$ cost. Therefore, the overall training complexity of the Volterra equalizer is dominated by $O(TM^{2p} + M^{3p})$.

In the model-driven RC, the feature dimension D is defined by the number of virtual nodes N_v. The readout weights $\bar{\mathbf{W}}_{\text{out}}$, calculated using (7), require matrix multiplication with a computational complexity of $O(TN_v^2)$ and matrix inversion with a complexity of $O(N_v^3)$. Therefore, the overall training complexity is dominated by $O(TN_v^2 + N_v^3)$.

However, the computational complexity of the DNN equalizer is analyzed separately due to its fundamentally different training paradigm. The complexity is evaluated in terms of multiply–accumulate operations (MACs), where P denotes the number of trainable parameters per subcarrier, T represents the total number of training samples, and E denotes the number of training epochs. Since each training sample only activates the parameters associated with its corresponding subcarrier, the per-sample computational cost consists of P MACs for the forward pass, $2P$ MACs for backpropagation, and an additional constant cost of 4 MACs for the forward and backward evaluation of the MSE loss. The computational cost associated with the activation functions is neglected, as it is marginal compared with the dominant MAC operations. By summing over all training samples and epochs, the total training complexity of the DNN equalizer is given by $O(TE(3P + 4))$.

The computational complexity is concretely evaluated using the optimized parameters specified in Section III, accounting for both the feature generation process and the subsequent LS based weight regression. For $T = 7560$ effective training samples, corresponding to 120 OFDM symbols, the total training complexity of the traditional RC is approximately 18,564,875 MACs. For the Volterra equalizer with $p = 2$ and $M = 5$, the resulting feature dimension is $D = 20$, leading to a total training cost of 3,183,200 MACs. For the proposed model-driven RC with $N_v = 6$, the total training complexity, including LED-based feature generation, frequency-domain transformation, and LS-based weight regression, is 1,176,174 MACs. For the DNN equalizer, with $E = 30$ and $P = 4$, the training complexity corresponds to approximately 3,628,800 MACs.

To establish a complete system level comparison, the mandatory FFT overhead required for OFDM demodulation is further taken into account. Each received OFDM symbol requires one FFT operation, incurring approximately 4,480 MACs per symbol. Consequently, for the 120 training OFDM symbols, this common preprocessing cost amounts to 537,600 MACs for the traditional RC and the Volterra equalizers. This FFT cost is independent of the equalization algorithm and therefore represents a shared system-level overhead rather than an algorithm-specific computation. Similarly, the DNN equalizer uses the real and imaginary parts of the OFDM symbols as input and thus also requires the same FFT-based demodulation preprocessing. In contrast, for the proposed model-driven RC, the frequency-domain processing is inherently integrated into the

TABLE III
COMPUTATIONAL COMPLEXITY OF DIFFERENT EQUALIZERS

Algorithm	Training Complexity	Inference Complexity (per step)
One-tap	$O(T + LN_{\text{fft}}\log_2(N_{\text{fft}}))$	$O\left(1 + \frac{N_{\text{fft}}}{N_{\text{sub}}}\log_2(N_{\text{fft}})\right)$
Volterra	$O(TM^{2p} + M^{3p} + LN_{\text{fft}}\log_2(N_{\text{fft}}))$	$O\left(M^p + \frac{N_{\text{fft}}}{N_{\text{sub}}}\log_2(N_{\text{fft}})\right)$
Traditional RC	$O(TN_r^2 + N_r^3 + LN_{\text{fft}}\log_2(N_{\text{fft}}))$	$O\left(N_r^2 + \frac{N_{\text{fft}}}{N_{\text{sub}}}\log_2(N_{\text{fft}})\right)$
DNN	$O(TE(3P+4) + LN_{\text{fft}}\log_2(N_{\text{fft}}))$	$O\left(P + \frac{N_{\text{fft}}}{N_{\text{sub}}}\log_2(N_{\text{fft}})\right)$
Model-driven RC	$O(TN_v^2 + N_v^3 + TN_v\log_2(N_v))$	$O(N_v + N_v\log_2(N_v))$

feature generation stage, and the corresponding FFT-related cost has already been included in the reported training complexity.

The inference complexity includes core equalization operations and the mandatory FFT cost for OFDM demodulation. The FFT cost contributes a fixed cost of $O(\frac{1}{N_{\text{sub}}}N_{\text{fft}}\log_2(N_{\text{fft}}))$ for each QAM symbol at the effective subcarrier. In addition to this cost, the complexities of the different equalizers are as follows. For the traditional RC reservoir update, the complexity is $O(N_r^2)$. For the Volterra equalizer polynomial evaluation, the complexity is $O(M^p)$. For the DNN equalizer, only P multiply–accumulate operations are required per subcarrier, resulting in an inference complexity of $O(P)$. For the model-driven RC, the complexity is $O(N_v + N_v\log_2(N_v))$ due to the combination of scalar recursions and additional FFT cost, which involve transforming from the time domain to the frequency domain without requiring additional OFDM demodulation cost.

Table III summarizes these asymptotic complexity results. In the table, L denotes the number of OFDM symbols used for training. The comparison demonstrates that the proposed model-driven RC achieves substantially lower computational complexity than both the traditional RC and the Volterra equalizer.

IV. CONCLUSION

This paper has presented an LED model-driven RC equalizer for OFDM-VLC systems, demonstrating consistently superior performance and robustness compared with conventional equalizers. The proposed approach achieves a 34.6% and 56.0% BER reduction compared to Volterra and traditional RC algorithms, respectively. It also demonstrates higher achievable rates, particularly under high-bandwidth conditions, and greater data efficiency, reaching optimal performance with only 20% of the available training data, while other algorithms require approximately 50%. Furthermore, the model-driven RC exhibits improved generalization capability, maintaining strong performance even under sudden channel degradation. Computational complexity analysis shows that the model-driven RC offers a more favorable performance complexity trade-off, with lower training and inference costs than both Volterra and traditional RC, while preserving superior BER and SNR performance. In addition, when compared with a lightweight DNN equalizer of comparable complexity, the proposed model-driven RC consistently achieves better BER and SNR performance, highlighting the advantage of incorporating physical modeling into the learning framework. These results highlight the practicality and efficiency of the model-driven RC for real VLC deployments, particularly in challenging conditions with limited training data and pronounced nonlinear distortion.

REFERENCES

[1] P. Yang, Y. Xiao, M. Xiao, and S. Li, "6G wireless communications: Vision and potential techniques," *IEEE Netw.*, vol. 33, no. 4, pp. 70–75, Jul./Aug. 2019.

[2] L. Yin, W. O. Popoola, X. Wu, and H. Haas, "Performance evaluation of non-orthogonal multiple access in visible light communication," *IEEE Trans. Commun.*, vol. 64, no. 12, pp. 5162–5175, Dec. 2016.

[3] T. Huang, W. Yang, J. Wu, J. Ma, X. Zhang, and D. Zhang, "A survey on green 6G network: Architecture and technologies," *IEEE Access.*, vol. 7, pp. 175758–175768, 2019.

[4] X. Huang et al., "2.0-Gb/s visible light link based on adaptive bit allocation OFDM of a single phosphorescent white LED," *IEEE Photon. J.*, vol. 7, no. 5, Oct. 2015, Art. no. 7904008.

[5] S. Niu, P. Wang, S. Chi, Z. Liu, W. Pang, and L. Guo, "Enhanced optical OFDM/OQAM for visible light communication systems," *IEEE Wireless Commun. Lett.*, vol. 10, no. 3, pp. 614–618, Mar. 2021.

[6] J. He, J. He, and J. Shi, "An enhanced adaptive scheme with pairwise coding for OFDM-VLC system," *IEEE Photon. Technol. Lett.*, vol. 30, no. 13, pp. 1254–1257, Jul. 2018.

[7] W. W. Hu, "PAPR reduction in DCO-OFDM visible light communication systems using optimized odd and even sequences combination," *IEEE Photon. J.*, vol. 11, no. 1, Feb. 2019, Art. no. 7901115.

[8] T. Zhang, Y. Zou, J. Sun, and S. Qiao, "Improved companding transform for PAPR reduction in ACO-OFDM-based VLC systems," *IEEE Commun. Lett.*, vol. 22, no. 6, pp. 1180–1183, Jun. 2018.

[9] D. Sun et al., "6 Gbps micro-LED transmission using OFDM with predistortion and single-tap nonlinearity compensation," *IEEE Photon. Technol. Lett.*, vol. 35, no. 14, pp. 781–784, Jul. 2023.

[10] Z. Li and C. Zhang, "An improved FD-DFE structure for downlink VLC systems based on SC-FDMA," *IEEE Commun. Lett.*, vol. 22, no. 4, pp. 736–739, Apr. 2018.

[11] R. Mitra and V. Bhatia, "Adaptive sparse dictionary-based kernel minimum symbol error rate post-distortion for nonlinear LEDs in visible light communications," *IEEE Photon. J.*, vol. 8, no. 4, Aug. 2016, Art. no. 7905413.

[12] G. Stepniak, J. Siuzdak, and P. Zwierko, "Compensation of a VLC phosphorescent white LED nonlinearity by means of Volterra DFE," *IEEE Photon. Technol. Lett.*, vol. 25, no. 16, pp. 1597–1600, Aug. 2013.

[13] Y. Wang, L. Tao, X. Huang, J. Shi, and N. Chi, "8-Gb/s RGBY LED-based WDM VLC system employing high-order CAP modulation and hybrid post equalizer," *IEEE Photon. J.*, vol. 7, no. 6, Dec. 2015, Art. no. 7904507.

[14] C. Ye, D. Zhang, X. Hu, X. Huang, H. Feng, and K. Zhang, "Recurrent neural network (RNN) based end-to-end nonlinear management for symmetrical 50 Gbps NRZ PON with 29 dB loss budget," in *Proc. 2018 Eur. Conf. Opt. Commun.*, 2018, pp. 1–3.

[15] B. Karanov, Domaniç Lavery, P. Bayvel, and L. Schmalen, "End-to-end optimized transmission over dispersive intensity-modulated channels using bidirectional recurrent neural networks," *Opt. Exp.*, vol. 27, no. 14, pp. 19650–19663, 2019.

[16] C. He and S. Collins, "Signal demodulation using a radial basis function neural network (RBFNN) in a silicon photomultiplier-based visible light communication system," *IEEE Photon. J.*, vol. 14, no. 4, Aug. 2022, Art. no. 7337814.

[17] B. Lin, Q. Lai, Z. Ghassemlooy, and X. Tang, "A machine learning based signal demodulator in NOMA-VLC," *IEEE J. Lightw. Technol.*, vol. 39, no. 10, pp. 3081–3087, May 2021.

[18] W. Costa et al., "Toward AI-enhanced VLC systems for industrial applications," *IEEE J. Lightw. Technol.*, vol. 41, no. 4, pp. 1064–1076, Feb. 2023.

[19] A. Mohamed, A. S. Tag Eldien, M. M. Fouda, and R. S. Saad, "LSTM-Autoencoder deep learning technique for PAPR reduction in visible light communication," *IEEE Access.*, vol. 10, pp. 113028–113034, 2022.

[20] K. W. S. Palitharathna, N. D. Wickramasinghe, A. M. Vegni, and H. A. Suraweera, "Neural network-based optimization for SLIPT-enabled indoor VLC systems with energy constraints," *IEEE Trans. Green Commun. Netw.*, vol. 8, no. 2, pp. 839–851, Jun. 2024.

[21] Z. Lu et al., "11.2 Gbps 100-meter free-space visible light laser communication utilizing bidirectional reservoir computing equalizer," *Opt. Exp.*, vol. 31, no. 26, Dec. 2023, Art. no. 44315.

[22] K. Vandoorne et al., "Experimental demonstration of reservoir computing on a silicon photonics chip," *Nature Commun.*, vol. 5, no. 1, 2014, Art. no. 3541.

[23] A. Lugnan, S. Biasi, A. Foradori, P. Bienstman, and L. Pavesi, "Reservoir computing with all-optical non-fading memory in a self-pulsing microresonator network," *Adv. Opt. Mater.*, vol. 13, 2025, Art. no. 2403133.
[24] A. Katumba, X. Yin, J. Dambre, and P. Bienstman, "A neuromorphic silicon photonics nonlinear equalizer for optical communications with intensity modulation and direct detection," *J. Lightw. Technol.*, vol. 37, no. 10, pp. 2232–2239, May 2019.
[25] F. Da Ros, S. M. Ranzini, H. Bulow, and D. Zibar, "Reservoir-computing based equalization with optical pre-processing for short-reach optical transmission," *IEEE J. Sel. Topics Quantum Electron.*, vol. 26, no. 5, Sep./Oct. 2020, Art. no. 7701912.
[26] L. Appeltant et al., "Information processing using a single dynamical node as complex system," *Nature Commun.*, vol. 2, no. 1, 2011, Art. no. 468.
[27] J. Vatin, D. Rontani, and M. Sciamanna, "Experimental reservoir computing using VCSEL polarization dynamics," *Opt. Exp.*, vol. 27, no. 13, Jun. 2019, Art. no. 18579.
[28] F. D.-L. Coarer et al., "All-optical reservoir computing on a photonic chip using silicon-based ring resonators," *IEEE J. Sel. Topics Quantum Electron.*, vol. 24, no. 6, Nov./Dec. 2018, Art. no. 7600108.
[29] Y. Wei, M.-M. Zhao, and M.-J. Zhao, "Channel distribution learning: Model-driven GAN-based channel modeling for IRS-aided wireless communication," *IEEE Trans. Commun.*, vol. 70, no. 7, pp. 4482–4497, Jul. 2022.
[30] Z. Li et al., "Model-driven deep-learning for end-to-end optimization in fiber-terahertz communication systems," *J. Lightw. Technol.*, vol. 43, no. 7, pp. 3099–3117, Apr. 2025.
[31] J. Han et al., "Model-driven learning for physical layer authentication in dynamic environments," *IEEE Commun. Lett.*, vol. 28, no. 3, pp. 572–576, Mar. 2024.
[32] Y. Huang et al., "Reservoir computing based on LED model for signal equalization in VLC-OFDM system," in *Proc. 2024 Asia Commun. Photon. Conf.; Int. Conf. Inf. Photon. Opt. Commun.*, Beijing, China, Nov. 2024, pp. 1–4.
[33] Y. Zang et al., "Principle-driven fiber transmission model based on PINN neural network," *J. Lightw. Technol.*, vol. 40, no. 2, pp. 404–414, Jan. 2022.
[34] P. Zhu, H. Wang, and Y. Ji, "Security performance enhancement chaotic optical communication system based on reservoir computing for physical-layer security," *J. Lightw. Technol.*, vol. 42, no. 24, pp. 8628–8639, Dec. 2024.
[35] X. Deng et al., "Mitigating LED nonlinearity to enhance visible light communications," *IEEE Trans. Commun.*, vol. 66, no. 11, pp. 5593–5607, Nov. 2018.
[36] P. Zhu, H. Wang, and Y. Ji, "Ultra-high complexity optical VCSEL chaos generation based on reservoir computing and logistic map cascade for multiple applications," *J. Lightw. Technol.*, vol. 43, no. 14, pp. 6495–6507, Jul. 2025.
[37] Y. Wang, L. Tao, X. Huang, J. Shi, and N. Chi, "Enhanced performance of a high-speed WDM CAP64 VLC system employing Volterra series-based nonlinear equalizer," *IEEE Photon. J.*, vol. 7, no. 3, Jun. 2015, Art. no. 7901907.
[38] Y. Dong et al., "Equalization of short-reach IMDD transmission with enhanced reservoir computing," *J. Lightw. Technol.*, vol. 43, no. 3, pp. 1212–1221, Feb. 2025.
[39] G. Donati, C. R. Mirasso, M. Mancinelli, L. Pavesi, and A. Argyris, "Microring resonators with external optical feedback for time delay reservoir computing," *Opt. Exp.*, vol. 30, no. 1, pp. 522–537, Jan. 2022.
[40] S. Mardanikorani, X. Deng, and J.-P. M. G. Linnartz, "Sub-carrier loading strategies for DCO-OFDM LED communication," *IEEE Trans. Commun.*, vol. 68, no. 2, pp. 1101–1117, Feb. 2020.
[41] X. Deng et al., "Two-dimensional power allocation for optical MIMO-OFDM systems over low-pass channels," *IEEE Trans. Veh. Technol.*, vol. 71, no. 7, pp. 7244–7257, Jul. 2022.